

Full-Wave Simulation of Body Absorption due to Radiated Fields at GHz Frequencies

Simulación Electromagnética de Absorción de Radiación Electromagnética en el rango GHz.

Jose Alberto Carballo-Madrigal¹, Heinz Dietrich Brüns²,
Renato Rimolo-Donadio³, Christian Schuster⁴

Fecha de recepción: 6 de agosto de 2017
Fecha de aprobación: 18 de noviembre de 2017

Carballo-Madrigal, J; Brüns, H.D; Rimolo-Donadio, R;
Schuster, C. Full-Wave Simulation of Body Absorption due to
Radiated Fields at GHz Frequencies. *Tecnología en Marcha*.
Vol. 31-2. Abril-Junio 2018. Pág 171-181.

DOI: 10.18845/tm.v31i2.3634



- 1 Escuela de Ingeniería Electrónica, Instituto Tecnológico de Costa Rica. Costa Rica. Correo electrónico: jcarballomadrigal@gmail.com.
- 2 Hamburg University of Technology (TUHH). Germany.
- 3 Escuela de Ingeniería Electrónica, Instituto Tecnológico de Costa Rica. Costa Rica.
- 4 Institute of Electromagnetic Theory, Hamburg University of Technology (TUHH). Germany..

Palabras clave

Bioelectromagnetismo; Electromagnetismo Computacional; Método de Elementos Finitos; Método de Integración Finita; Métodos de los Momentos; Tasa de Absorción Específica.

Resumen

La exposición humana a radiaciones no ionizantes en alta frecuencia se ha vuelto común debido a la gran cantidad de sistemas que operan en ese rango, tales como teléfonos celulares, redes inalámbricas de datos y sistemas de comunicación en general. Modelar el impacto de este tipo de radiaciones es importante debido a los potenciales riesgos a la salud humana a corto y largo plazo, así como para la definición de límites de seguridad. Desde la perspectiva de la simulación numérica, esto es una tarea difícil debido a que las longitudes de onda asociadas son mucho más pequeñas que la dimensión típica del cuerpo humano, lo que resulta en un requerimiento de discretización muy fina de los modelos geométricos, con una consecuente alta demanda en los recursos de computación y largos tiempos de ejecución.

En este artículo se estudia la factibilidad de realizar simulaciones de onda completa para estimar el campo electromagnético absorbido en alta frecuencia, hasta 10 GHz, con solucionadores numéricos de propósito general y geometrías con tamaños relevantes en relación al tamaño del cuerpo humano. Geometrías simples son analizadas, definiendo las propiedades del agua fresca para su región interna. Tres diferentes métodos son evaluados: el método de integración finita (FIT), el método de elementos finitos (FEM) y el método de los momentos (MoM), con la intención de determinar la convergencia del resultado y los recursos computacionales necesarios en cada caso. Los resultados indican que a 10 GHz se torna difícil realizar dichos análisis con un recurso computacional moderado (hasta 64 GB RAM), pero algunas aproximaciones podrían ser explotadas debido a que la penetración del campo en ese rango de frecuencias esta principalmente acotada a la región cercana a la superficie del objeto.

Keywords

Bioelectromagnetism; Computational Electromagnetics; Finite Integration Technique; Finite Element Method; Method of Moments; Specific Absorption Rate.

Abstract

Exposition of humans to non-ionizing radiation at high frequencies has become ubiquitous due to the higher number of systems operating in that frequency range such as cell phones, wireless networks, and communication systems. The modeling of the impact of this type of radiation is an important issue due to potential short and long-term health effects and for the establishment of regulatory safety limits. From the simulation point of view, this is a challenging task since the wavelengths of interest are much smaller than the typical dimensions of a human body, which leads to the requirement of very fine discretization of the geometrical models and the consequent high demand of computational resources and long execution times.

This article studies the feasibility of a full-wave simulation of field absorption at high frequencies, up to 10 GHz, with general purpose numerical methods and geometries with sizes in the order of a human body. Simple geometries are analyzed, assuming the material properties of fresh water for their inner region. Three different methods are evaluated: the finite integration technique (FIT), finite element method (FEM), and method of moments (MoM), to determine the result convergence and required computational resources for each solution. The results show that already at 10 GHz it is difficult to perform the analysis with moderate computational power (up to 64 GB RAM), but some approximations might be exploited since field penetration in that frequency range is mostly limited to the surface region.

Introduction

Research work on exposure of humans to electromagnetic non-ionizing radiation has been a subject of interest due to the short and long-term health concerns and the higher amounts of exposure caused by emerging technologies that emit such type of radiation. See, for instance, [1], [2]. Even though health effects for ionizing radiation and high-power fields are well known, e.g. [1], [3], long-term effects from exposure to EM radiation are not so well understood [4]-[5]. The calculation and analysis of the specific absorption rate (SAR) have been used as a metric to assess the amount of energy absorbed by humans from the exposure of electromagnetic radiation [1]. SAR is also useful to define safety radiation limits for non-ionizing and low-power fields. Nevertheless, the SAR evaluation at frequencies in the Gigahertz range has not been explored in detail, partially due to the complications associated with high-frequency measurements and the difficulties to simulate geometries that are much larger than the wavelength.

To evaluate the capabilities of general purpose full-wave solvers to estimate field absorption in the GHz range, this work presents an analysis comparing three different methods: Method of Moments with the CONCEPT-II solver [6], Finite Integration Technique (FIT) with the Microwave Studio solver [7], and the Finite Element Method (FEM) with the HFSS solver [8].

The paper is organized as follows. First, a basic theoretical background is provided to support the analysis in the paper. Then, the geometrical models used in this work are described, and the results are compared and discussed. Finally, most important conclusions and perspectives for further work are addressed. This article presents part of the work developed as the final graduation project for the Licentiate Degree in Electronic Engineering called “Evaluation of the MOM for the computation of SAR” [9].

Theoretical Background

Computational electromagnetics, known as CEM, deals with the numerical approximated solution of Maxwell’s equations to calculate electric and magnetic fields in presence of arbitrary geometries and material definitions. Many different alternatives and methods to electromagnetic simulation are available, each of them showing advantages and disadvantages to solve certain types of problems. The techniques under study in this work are FIT, see e.g. [10], FEM, see e.g. [11], and MoM, see e.g. [12]. The first two methods are volume methods, which require full discretization of the computational domain, whereas the last one is a surface method that focuses on the discretization on the outer shell of the conductive regions. As a general perspective of the main differences among the basic formulation of each method, table I shows the main features of each approach.

Table 1. Comparison between FIT, FEM, and MoM as numerical techniques

Formulation	Equation Type	Solution Domain	Discretization Approach
FIT	Integral	Time	Volume
FEM	Differential	Frequency	Volume
MoM	Integral	Frequency	Surface

Time varying electromagnetic fields can be described in terms of travelling waves. The characteristics of those waves are dependent on the emitting source and the properties of the media where they propagate. The temporal frequency (f), the wavelength (or spatial period, λ), and the propagation velocity (v_p) of a wave are related by the fundamental equation:

$$v_p = \lambda \cdot f \quad (1)$$

In the GHz frequency range, for instance, plenty of commercial wireless standards have become ubiquitous at homes and workplaces; short-reach wireless networks often work in frequency bands around 2.4 and 5 GHz [13]. Considering electromagnetic propagation in free space, the propagation velocity of waves approaches the speed of light ($c \approx 2.99 \cdot 10^8$ m/s).

For the frequency range of this work, from 1 up to 10 GHz and according to (1), the free space wavelengths will be among 30 cm and 3 cm, respectively. If the media is other than free space, the propagation velocity will decrease depending on the properties of the material. For instance, considering fresh water as a homogeneous material with a relative dielectric constant of 78, the propagation velocity will become $c/(\epsilon_r)^{0.5} = 0.33 \times 10^8$ m/s. This translates to a wavelength range of about 3 cm to 3 mm for the same frequency interval of 1 to 10 GHz.

It is therefore important to note that this wavelength range is much smaller than the dimensions of a human body. A detailed full-wave simulation will require to discretize the model considering a fraction of the smallest wavelength of interest, a parameter known as lambda refinement. This criterion relates the element size in the mesh to the shortest wavelength and it will lead to a very large number of mesh elements for electrically large objects.

Since many biological tissues behave as bad conductors (conductive media with a moderate and non-negligible conductivity s), the skin effect needs to be considered [14]. The characteristic depth in the material at which waves can penetrate before being almost fully attenuated is given for non-magnetic materials by:

$$\delta = \sqrt{\frac{1}{\pi f \sigma \mu_0}} \quad (2)$$

The variable μ_0 represents the permeability of free space $4 \cdot \pi \cdot 10^{-7}$ H/m. The skin effect phenomena can be understood as the exponential decay of the fields when they penetrate the material, and it is proportional to the square root of frequency and the conductivity of the material as defined in (2). This means that the fields will be mostly confined to a region near to the surface of the material as frequency or conductivity increase.

As a metric to evaluate the field absorption, the specific absorption rate (SAR) is a quantity often used in relation to biological tissues. There are different standards and relationships to quantify SAR depending on the mass of the material and the distance from the body to the source [15]. The relation used in this investigation is the point SAR:

$$SAR_{Point} = \frac{\sigma(r) |E(r)|^2}{\rho(r)} \quad (3)$$

where $\sigma(r)$ is the conductivity of the material, $\rho(r)$ is the mass density of the material, and $|E(r)|^2$ is the squared magnitude of the electric field (E-field), as a function of the position r . Since the models used in this work have constant conductivity and density, the results are evaluated in terms of the square magnitude of the E-field only.

Evaluation Cases for Computation of Field Absorption

Simple geometrical models were defined to be evaluated with the three methods, focusing on the required effort to obtain convergent results in all simulations. The procedure of comparison was to calculate the electric field inside the body along a probe line. Also, an analytical solution for the case of a sphere was used [16].

Another aspect to assess the quality of the results is the validation of expected physics. This can be carried out, for example, by 2D views of electric field distributions. Plots of the E-field behavior at different phases can reflect velocity of propagation, boundary condition enforcement, wavelength related maxima and minima, resonances, field penetration and distribution, among others.

The selection of the geometrical models is based on a strong simplification of human anatomy. In the first case, a sphere geometry allusive to the average adult human head size is considered [17]; for the second case, an ellipsoidal geometry is considered, with a size that resembles the whole body of an average adult [15].

The chosen excitation is a plane wave with the following features: linear polarization, propagation in the $x+$ direction, E vector polarized in $z+$ direction, and a real amplitude of 1 V/m. The polarization of the plane wave was defined as an approximation of the far-field radiation of a transmitter source.

The material modeling by itself is a vast topic in terms of tissue properties, its water content, polarization, and other related frequency dependent quantities as detailed in [1] and [18]. In this work, the material inside the model object is simplified to have the properties of fresh water, since it is the main component of biological tissue. The electrical properties of water can be found in [19], and the following values were used: relative permittivity of 78, relative permeability of 1, mass density of 1000 kg/m and a conductivity of 1.59 S/m, as detailed in [20].

As a general consideration, local and general mesh refinements were implemented in each specific framework. Also, the exploitation magnetic and electric symmetry to reduce the models to a quarter of its original size was applied, in order to reduce the number of unknowns and computational effort.

The definition and parameter summary for the sphere and ellipsoid models can be seen in figure 1 and table 2. The trajectories defined as AB and CD are lines constituted by a finite number of observation points or probes.

Table 2. Summary of the trajectories for the two geometries (Sphere: S and Ellipsoid: E)

Name	Length (cm)	From	To	Axis
AB-S	30	-15	15	X
AB-E	100	-50	50	X
CD-S	30	-15	15	Z
CD-E	200	-100	100	Z

Results and Analysis

Complete 3D solutions with the sphere and ellipsoid models were computed with the three solvers at frequencies ranging from 1GHz up to 10 GHz. To analyze the results in a more convenient way, field plots along lines and over 2D cuts are used for visualization and comparison purposes.

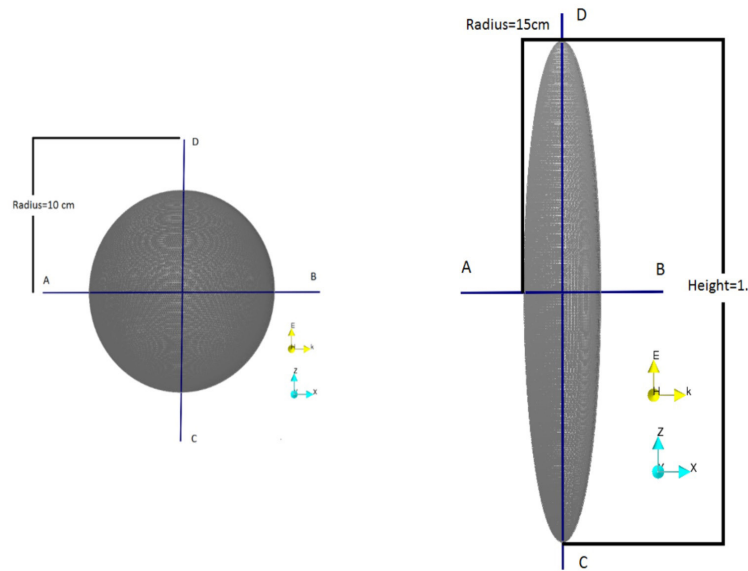


Figure 1. Sphere and Ellipsoid models. Trajectories AB and CD are shown. The yellow vectors represent the orientation of the excitation (plane wave), and the blue vectors represent coordinate system definition. The model (surface patch grids) were generated with CONCEPT-II.

Figures 2, 3 and 4 show field distributions for the sphere model, computed by MoM. Similar results could be achieved from other solvers. From figures 2 and 3, a comparison of the effect of increasing the frequency for the sphere model is illustrated. It is possible to see that the electric field behavior outside the model is quite different; note that different wavelengths are associated. Also, the wavelength related maximum and minima of the plane wave surrounding the sphere can be seen. The higher intensity spots, in red and yellow along the outer circumference, are more distant in figure 2 in comparison to Figure 3, which is the result of a longer outside wavelength at 1 GHz. The figures also show the field contrast between the inner region of the sphere and outer free space region at 1 GHz and 10 GHz, each for a constant phase of 0 degrees. It can be observed that although the strong damping in both cases, at 1 GHz still some fields are observed inside the sphere in the linear scale shown. This is not possible anymore with the linear scale at 10 GHz. Vortices inside the sphere and more intense circular fields at the center of the body are predicted by the analytical solution as well. These phenomena appear due to a superposition effect inside the body.

In figure 4, the equivalent current distribution over the surface of the sphere is depicted at 10 GHz. This shows that the portion of the body being directly illuminated by the plane wave is receiving most power from the source. This can be related to the field plots in previous figures; when the plane wave impacts the body, most energy travels along the surface and a strong damping inside the structure suggests that only a small portion of the energy is dissipated inside the body.

Figure 5 shows a comparison obtained from the simulations with the three codes and the analytical solution for the square of the E-field along a trajectory inside the sphere at 1 GHz. A good agreement of all curves including the analytical solution can be observed. The strong damping inside the body is expected, as mentioned before, due to the finite conductivity. Although the electric field values strongly drop, boundary conditions are fulfilled by preserving a continuous transition of the tangential E-fields at the air/dielectric interface.

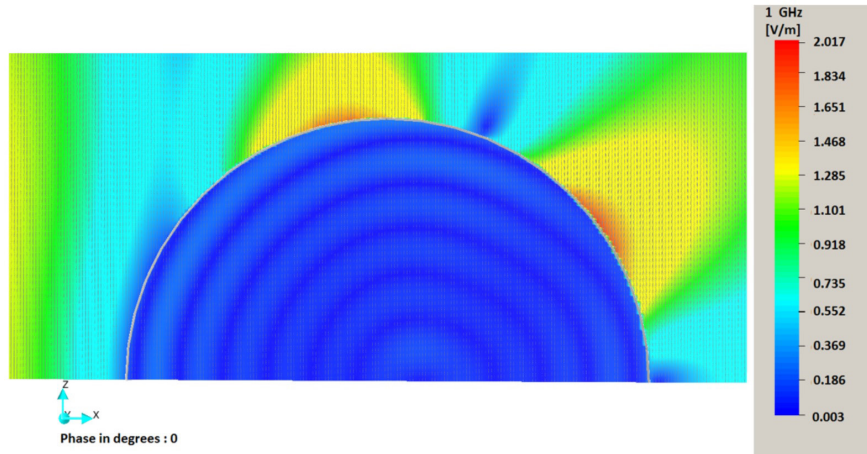


Figure 2. XZ cut-plane electric field behavior with the sphere model at 1 GHz, generated with CONCEPT-II.

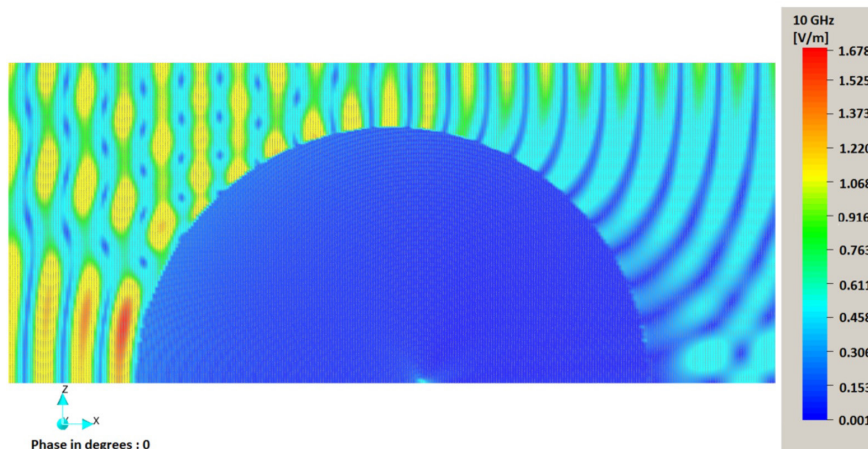


Figure 3. XZ cut-plane electric field behavior with the sphere model at 10 GHz, generated with CONCEPT-II.

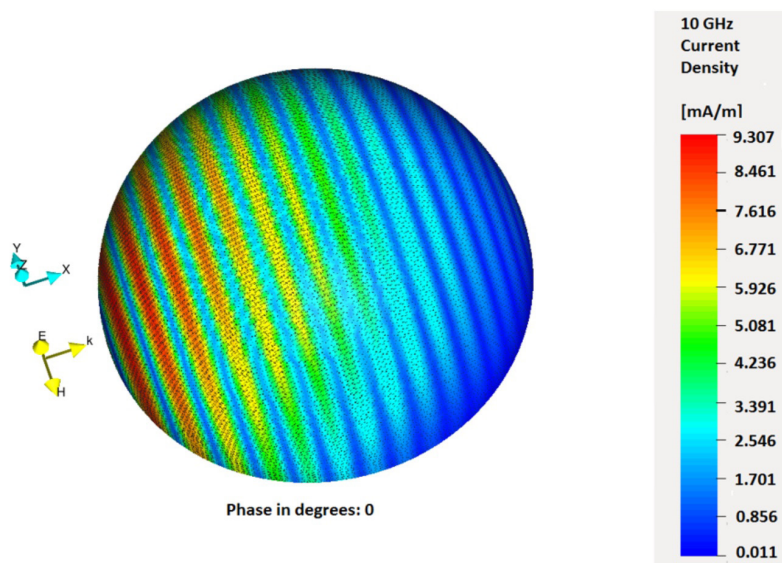


Figure 4. Current density on the sphere model illuminated by a plane wave at 10 GHz. Simulation result generated with CONCEPT-II. The current distribution responsible for the outside fields is shown at 0 degrees.

The result comparison at different frequencies is depicted in figure 6, obtained as an example, with the MoM code. Although the “resonance” at the center of the sphere is stronger at higher frequencies, the general trend is that the field is further damped inside the body as the frequency increases. This is consistent with the skin effect related behavior, which will predict less penetration as frequency increases. The standing wave pattern outside the sphere can be associated with reflections at the interface and the periodicity is associated with the wavelength of the incident wave.

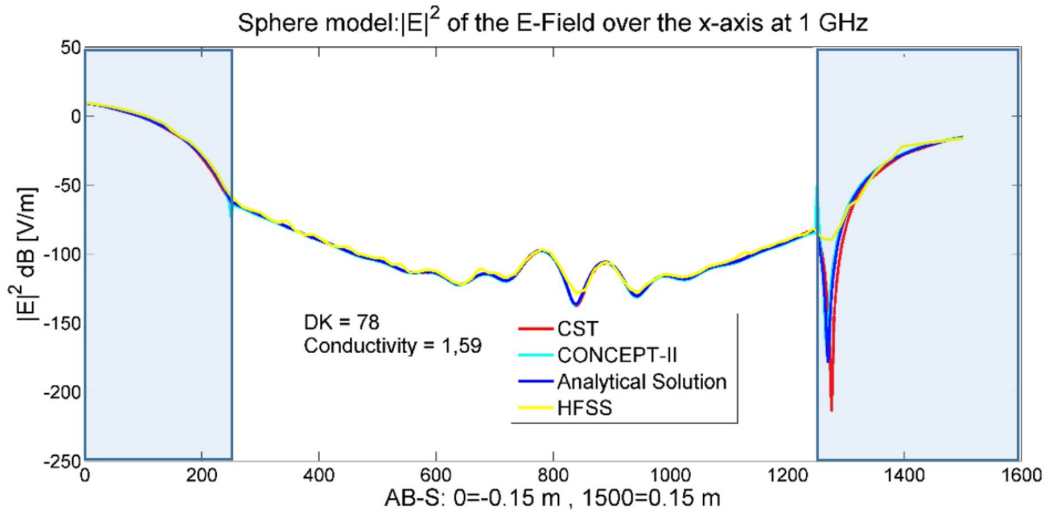


Figure 5. Electric field strength over the x-axis of the sphere at 1 GHz. The shaded parts indicate the outside region of the sphere.

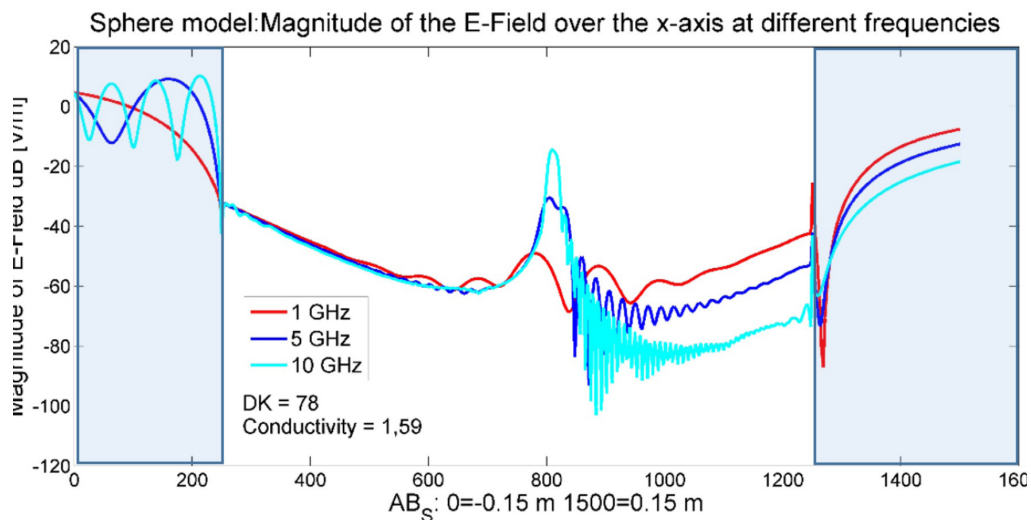


Figure 6. Electric field strength along the AB trajectory for the sphere at different frequencies. The shaded parts indicate the outside region of the sphere. Results obtained with CONCEPT1-II.

A selection of results for the simulations with the ellipsoid model are shown in figures 7 and 8. Figure 7 illustrates the E-field distribution in the XZ plane at 1 GHz. The results also predict a strong damping inside the body; the disappearance of a low-amplitude E-field concentration at the center of the body is observed in figure 8, in comparison to figure 2.

In figure 8, the electric field strength along a trajectory inside the ellipsoid is shown. It is possible to identify the high damping inside the body, increasing with frequency, and the reflection standing wave pattern on the external side where the plane wave illuminates the structure. Here, the highest field values in the body are located near to the surface, decreasing towards the center of the body. Similar results can also be found with the other methods in this case as well.

Table 3 shows the computational effort for each case and solver at different frequencies, where the main limitation with increasing frequency was the memory consumption. This is consistent with the fact that for shorter wavelengths, more mesh elements are required to satisfy the lambda related refinement in the simulations. Already with the simple geometries used in this work, long simulation times and large amounts of memory were required to reach the 10 GHz limit. Further simulation results are presented in [9].

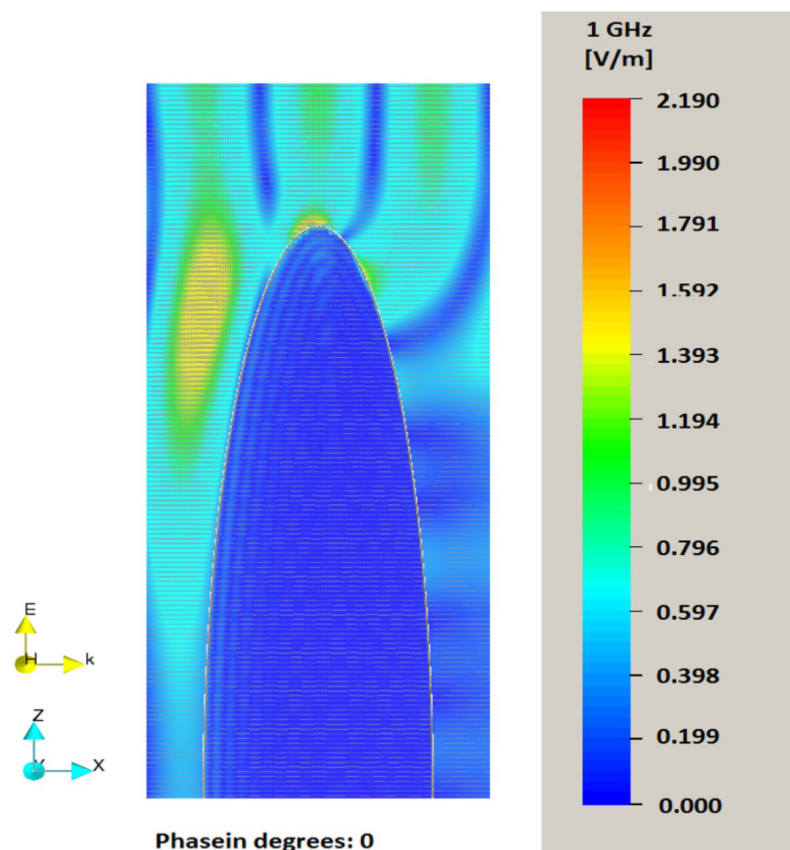


Figure 7. XZ cut-plane electric field behavior with the sphere model at 1 GHz, generated with CONCEPT-II.

As expected, MoM, as a surface (boundary element) method benefits from for this type of computation with a smaller number of discretization elements and shorter simulation times in comparison to volume methods (FEM, FIT). Although the memory usage is lower for MoM at lower frequencies, this advantage is not anymore present approaching 10 GHz. The fastest increase in computational demands with rising frequency was observed for the FEM technique, where the solutions could not be computed beyond 5 GHz with the available resources. It should be emphasized that there were growing and high memory demand for all methods at higher frequencies. With a more complex geometry (ellipsoid) the resource demand increases, which points towards an increasing difficulty to resolve complex geometries with sizes in the order of a human body in this frequency range.

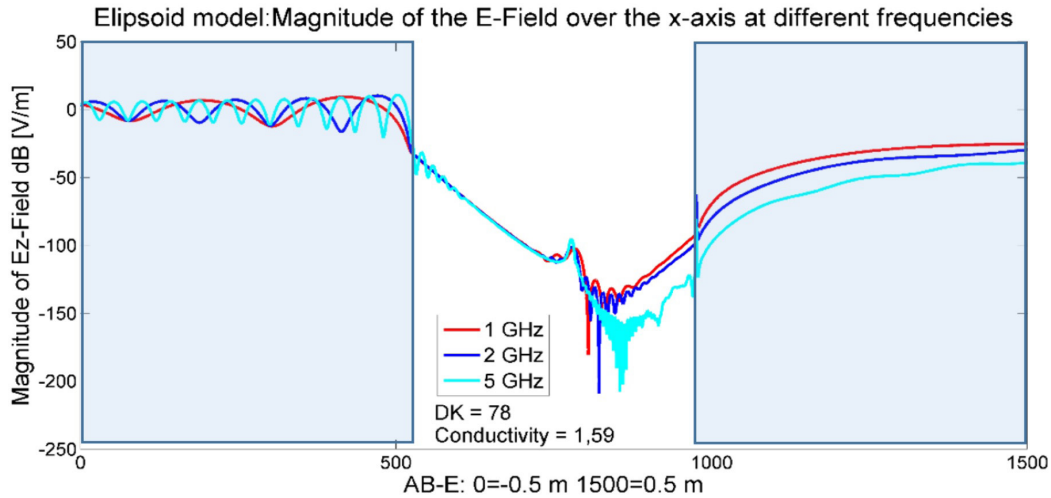


Figure 8. Electric field strength over the AB trajectory for the ellipsoid geometry. The shaded parts indicate the outside region of the sphere. Results obtained with CONCEPT-II.

Table 3. Comparison of computational resources for the evaluated tools

Software	Model	Frequency (GHz)	Number of elements	Comp. time (hh:mm:ss)	Memory (GB)
FIT	Sphere	1	698 296	00:01:09	0.31
		2	1 608 714	00:14:07	1.53
		5	31 049 568	02:53:41	12.31
		7	52 396 146	06:44:32	25.07
		10	66 772 496	14:10:29	31.74
MoM		1	1 028	00:00:05	0.02
		2	1 920	00:00:17	0.06
		5	11 966	00:02:27	2.13
		7	23 564	00:25:53	8.27
		10	47 466	01:05:32	34.38
FEM	1	17 873	00:00:51	1.01	
	2	69 047	00:05:41	9.92	
	5	326 563	01:30:00	40.90	
FIT	Ellipsoid	1	47 394 200	01:40:29	13.28
		3	185 558 145	05:36:35	31.68
MoM		1	10 990	00:17:50	1.80
		3	38 641	00:38:51	22.24
		5	68 558	03:06:40	70.03

Conclusions

Consistent simulation results could be achieved for field absorption in the GHz range with the three evaluated methods. From the physical perspective, all solutions are reliable with respect to electromagnetism requirements such as fulfillment of boundary conditions. Even though the

analyses were performed on simple geometries and homogeneous materials, computer resource demands increase quickly with the frequency of the analysis and become prohibitive reaching the 10 GHz limit used in this work. An advantage in terms of simulation time was observed with the MoM method, but the memory consumption scales quickly with frequency or the complexity of the geometry. Volume methods are associated with a larger number of elements and memory consumption at lower frequencies, for the FEM solver in particular.

The behavior observed in the studied cases resembles the expected behavior of a bad conductor material, considering the properties of water. A strong damping of fields inside the structure could be observed due to the skin effect in the GHz range, which is accentuated at higher frequencies. From the computational point of view, this means that to compute the full solution in all the regions might not be optimal and more efficient methods that concentrate the effort on regions near to the body surface might be more suitable for this type of problem.

References

- [1] T. Wu, T. S. Rappaport, and C. M. Collins. "Safe for Generations to Come: Considerations of Safety for Millimeter Waves in Wireless Communications," *IEEE Microwave Magazine*, vol. 16, no. 2, 2015, pp. 65-84.
- [2] G. Marin, G. Samoilescu, O. Baltag, and S. Radu. "Assessment of electromagnetic radiation exposure of embarked personnel on Romanian naval ships". In *Proc. International Conference and Exposition on Electrical and Power Engineering (EPE)*, 2014, pp.427-432.
- [3] IEEE Standards. "IEEE Standard for Safety Levels with Respect to Human Exposure to the Radio Frequency Electromagnetic Fields, 3 kHz to 300 GHz," IEEE Standard C95.1, 2007. [Available Online]: <http://standards.ieee.org/findstds/standard/C95.6-2002.html>
- [4] International Commission on Non-Ionizing Radiation Protection ICNIRP. "Guidelines for limiting exposure to time-varying electric, magnetic, and electromagnetic fields (up to 300 GHz)," *Health Phys.*, vol. 74, no. 4, 1998, pp. 494-522.
- [5] Federal Communications Commission (FCC). "Evaluating Compliance with FCC Guidelines for Human Exposure to Radiofrequency Electromagnetic Fields", Federal Communications Commission Standard, OFT Bulletin 65, Edition 97-01, 1997.
- [6] Electromagnetic Theory Institute, Technische Universität Hamburg (TET-TUHH). *CONCEPT-II*. [Available Online]: <http://www.tet.tu-harburg.de/concept/>, May 2017.
- [7] Computer Simulation Technology (CST). *Microwave Studio (MWS)*. [Available Online]: <http://www.cst.com>, April 2017.
- [8] ANSYS, *High Frequency Structure Simulator (HFSS)*. [Available Online]: <http://www.ansys.com>, April 2017.
- [9] J. Carballo-Madriral. "Evaluation of the MOM for the computation of Body Absorption," Instituto Tecnológico de Costa Rica, Electronics Engineering Lic. Thesis, Cartago, Costa Rica, June 2017.
- [10] M. Clemens and T. Weiland. "Discrete Electromagnetism with the Finite Integration Technique," *Progress in Electromagnetics Research, PIER* 32, 65-87, 2001.
- [11] D. Davidson, "Computational electromagnetics for RF and microwave engineering," 1st Ed. Cambridge: Cambridge University Press, 2005.
- [12] R. F. Harrington, "Field Computation by Moment Methods," New York, USA: Macmillan Co. 1968
- [13] IEEE Standards. "IEEE 802.11™: Wireless LANs." 2012 [Available online]: <http://standards.ieee.org/about/get/802/802.11.html>
- [14] C. A. Balanis. "Advanced Engineering Electromagnetics," 2 Ed., New York, USA: Wiley, 2012.
- [15] C. Furse, D. Christensen, and C. Durney. "Basic introduction to bioelectromagnetics," 1st Ed. Boca Raton, Florida, USA: CRC Press, 2009.
- [16] T. Mader. „Berechnung elektromagnetischer Felderscheinungen in abschnittweise homogen Medium mit Oberflächenstromsimulation.“ Ph.D. Thesis, Technische Universität Hamburg (TUHH), 1992.
- [17] V. Stanković, D. Jovanović, D. Krstić, and N. Cvetković. "Electric field distribution and SAR in human head from mobile phones," in *Proc. 9th International Symposium on Advanced Topics in Electrical Engineering (ATEE)*, Bucharest, 2015, pp. 392-397.
- [18] S. Gabriel, R. W. Lau, and C. Gabriel. „The dielectric properties of biological tissues: III. Parametric models for the dielectric spectrum of tissues,” *Phys. Med. Biol.*, vol. 41, no. 11, 1996, p. 2271.
- [19] J. Ellison. *Water: A dielectric reference*, J. Molecular Liquids, vol. 68, 1996.
- [20] P. A. Hasgall, F. Di Gennaro, C. Baumgartner, E. Neufeld, M. C. Gosselin, D. Payne, A. Klingenböck, and N. Kuster. "IT'IS Database for thermal and electromagnetic parameters of biological tissues," Version 3.0, September 1st, 2015. DOI:10.13099/VIP21000-03-0.